Electronic Supplementary Material (ESI) for Catalysis Science & Technology.

Supporting Information

Selective Synthesis of Core-Shell Structured Catalyst χ-Fe_5C_2 Surrounded by Nanosized Fe_3O_4 for Conversion of Syngas to Liquid Fuels

Lei Tang, [a] Bai-Chuan Zhou, [a] Xi Liu, [b] Shuang Xu, [a] Jia Wang, [a] Wei Xu, [a] XiaoHao Liu, [c] Liwei Chen [b] and An-Hui Lu*, [a]

[a]State Key Laboratory of Fine Chemicals, Liaoning Key Laboratory for Catalytic Conversion of Carbon Resources, School of Chemical Engineering, Dalian University of Technology, Dalian 116024, P. R. China

[b]School of Chemistry and Chemical, In-situ Center for Physical Science, Shanghai Jiao Tong University, Shanghai 200240, P. R. China

[c]Department of Chemical Engineering, School of Chemical and Material Engineering, Jiangnan University, Wuxi 214122, P. R. China

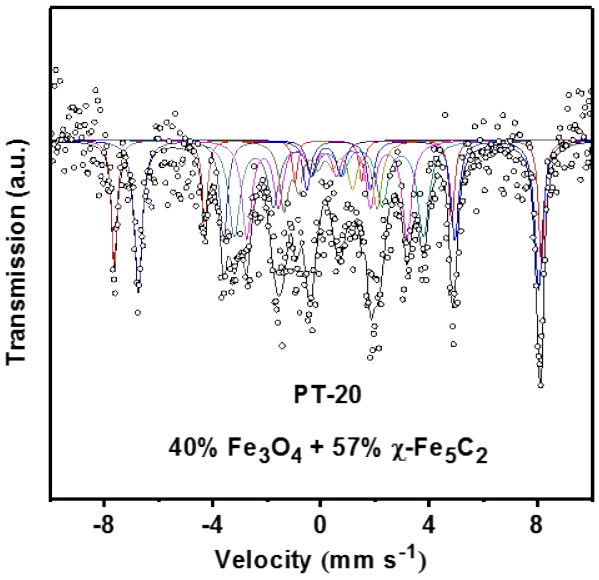

Figure S1. Mössbauer spectrum (MES) measured at room temperature of the PT-20 catalyst.

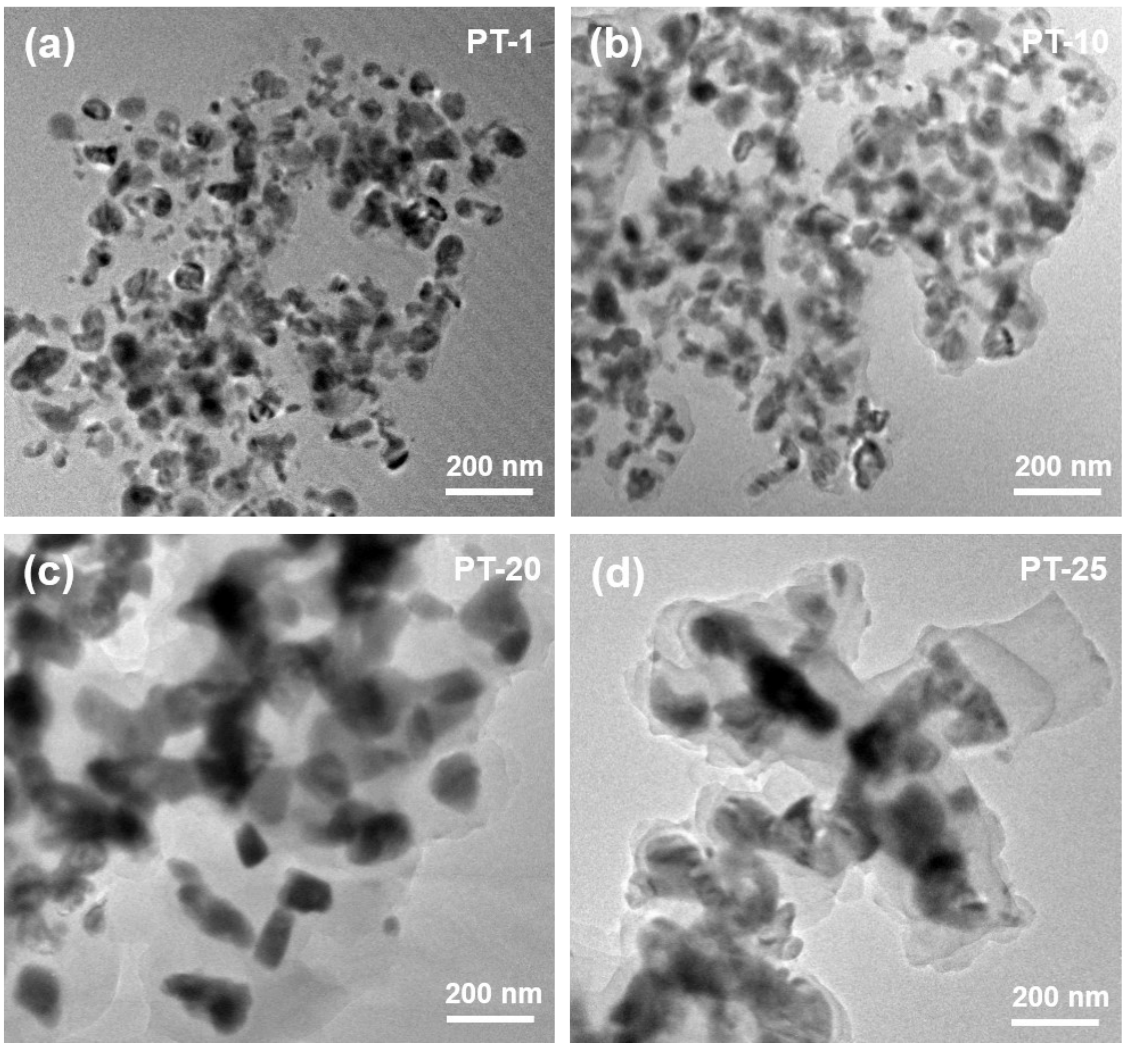

Figure S2. TEM images of pretreated (a) PT-1, (b) PT-10, (c) PT-20 and (d) PT-25 catalysts.

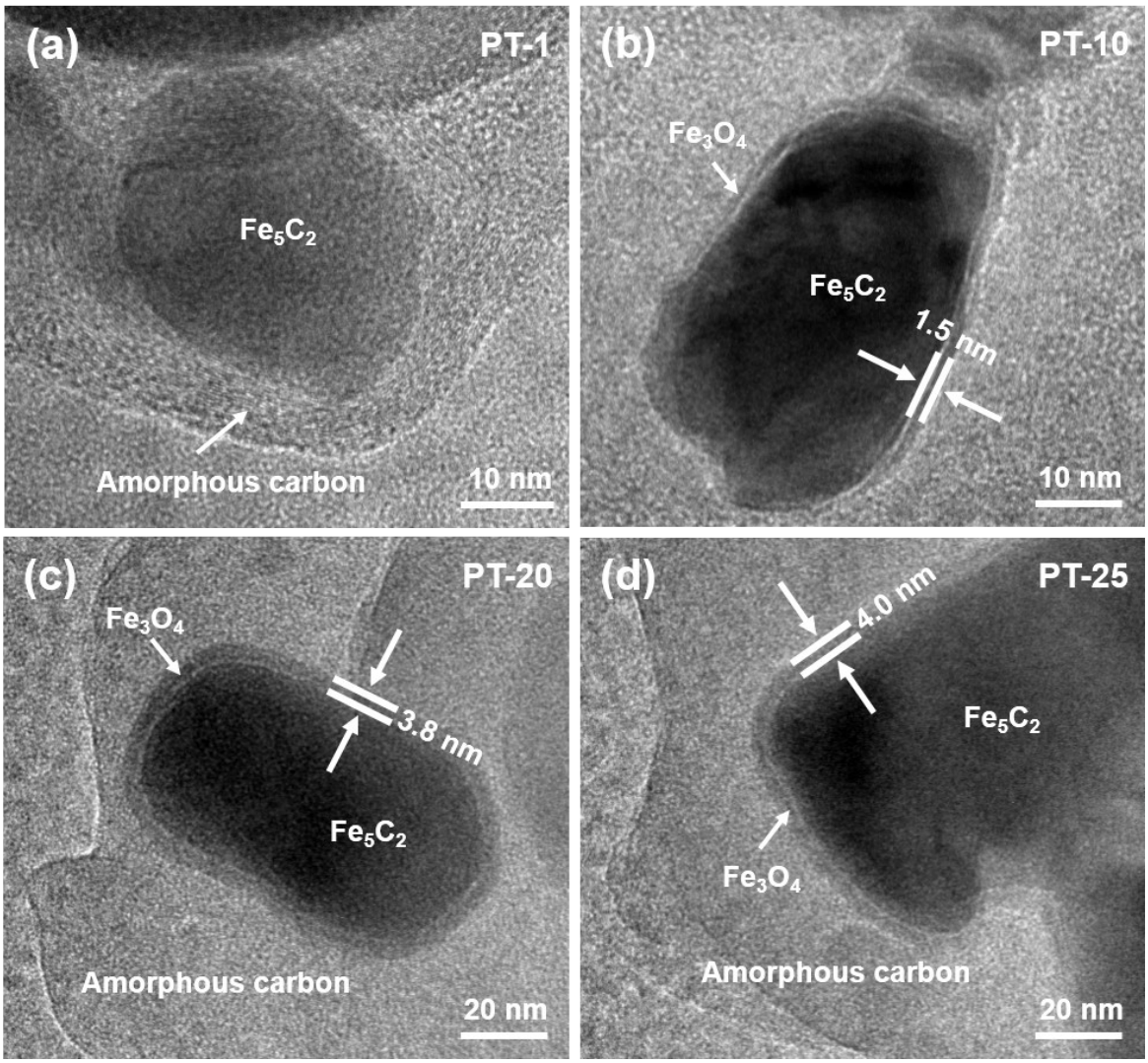

Figure S3. TEM images of pretreated (a) PT-1, (b) PT-10, (c) PT-20 and (d) PT-25 catalysts.

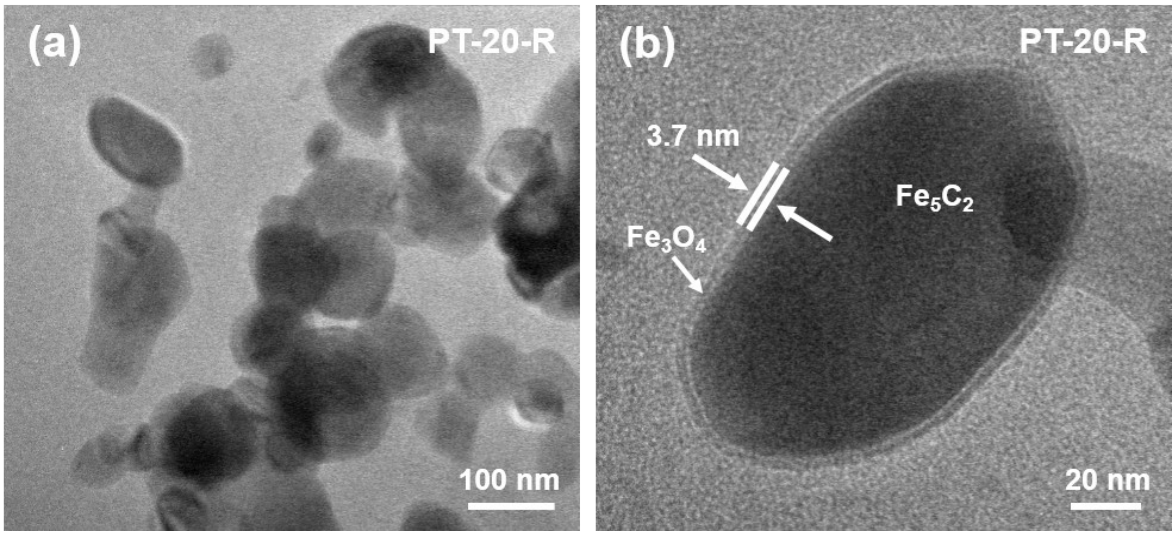

Figure S4. TEM images of the PT-20 catalyst after FTS reaction for 40 h.

The XRD patterns (Figure 1b) show that the diffraction peaks of the reacted catalysts retain well after FTS reaction for 40 h. Moreover, the TEM images of the reacted PT-20 catalyst are similar with those of the pretreated PT-20 catalyst, suggesting the catalysts retain stable during FTS reaction. This is also indicated by a stable CO conversion for the PT-20 catalyst is also observed during FTS reaction for 40 h.

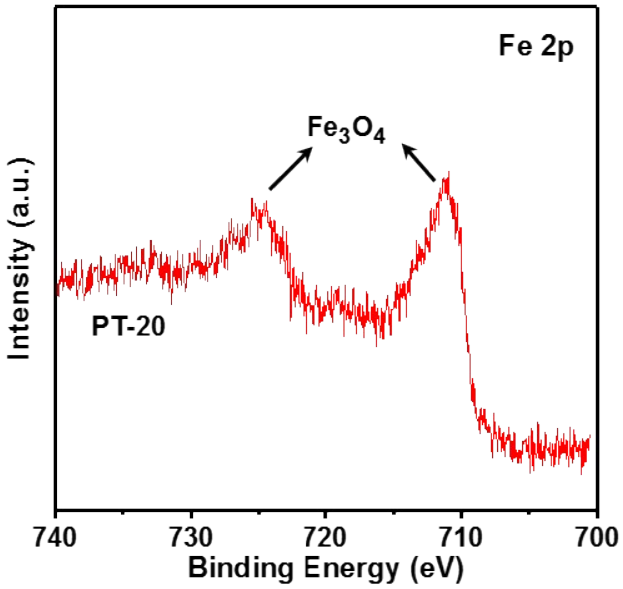

Figure S5. Fe 2p XP spectrum of the pretreated PT-20 catalyst.

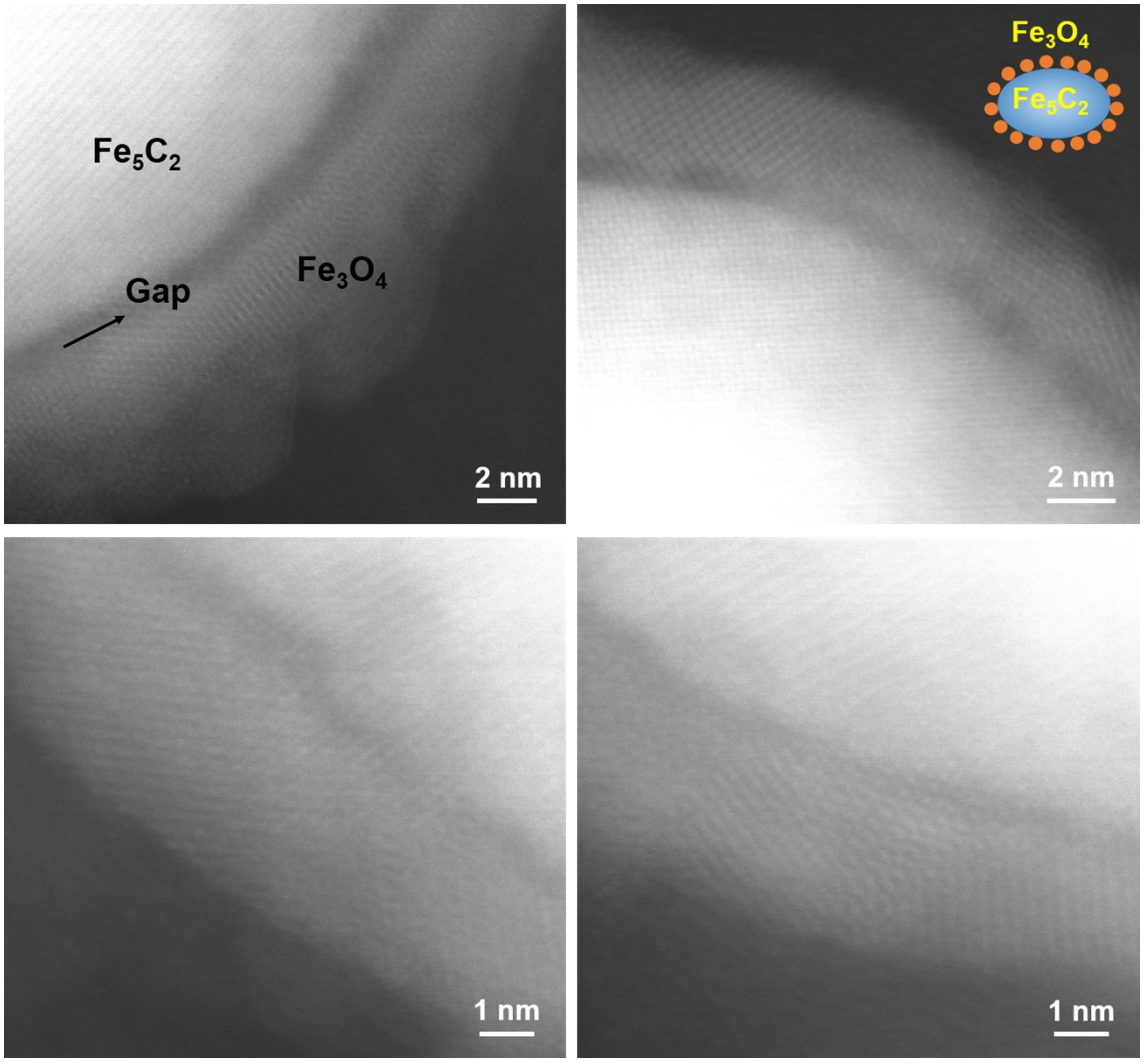

Figure S6. STEM-ADF images of typical areas of the pretreated PT-20 catalyst.

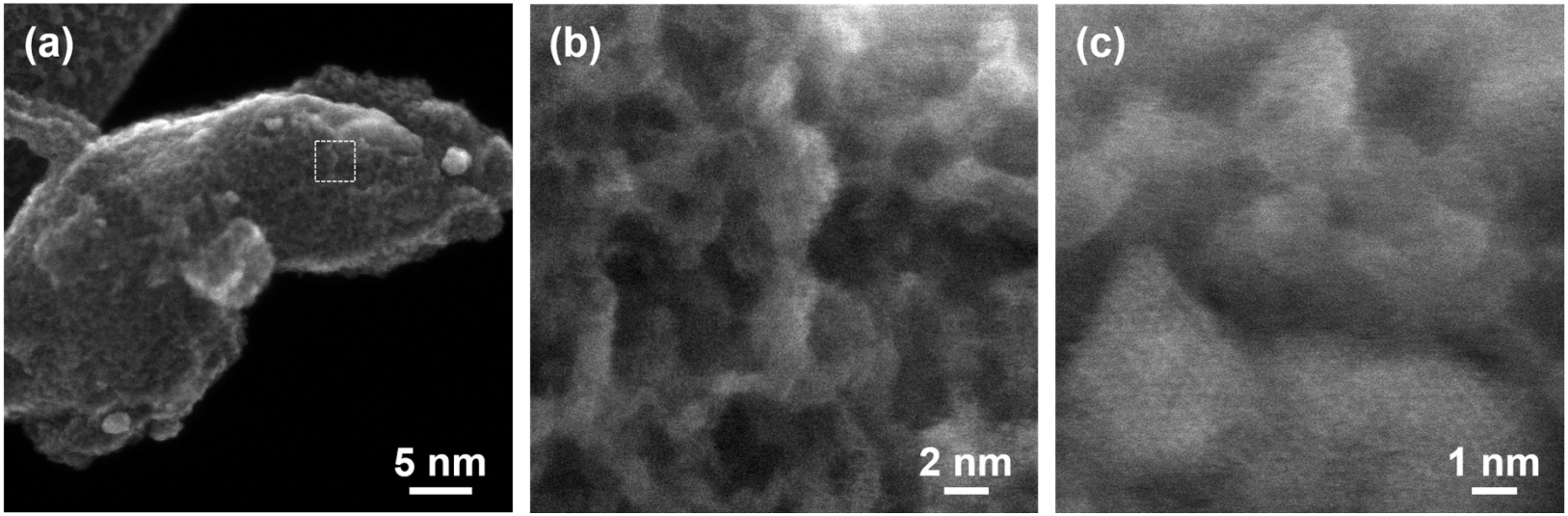

Figure S7. (a) STEM-SE images of the pretreated PT-20 catalyst, (b) high-resolution SE image of the region in the white square box in (a), and (c) atomically resolved SE images, showing the stacking structure of the oxide shell.

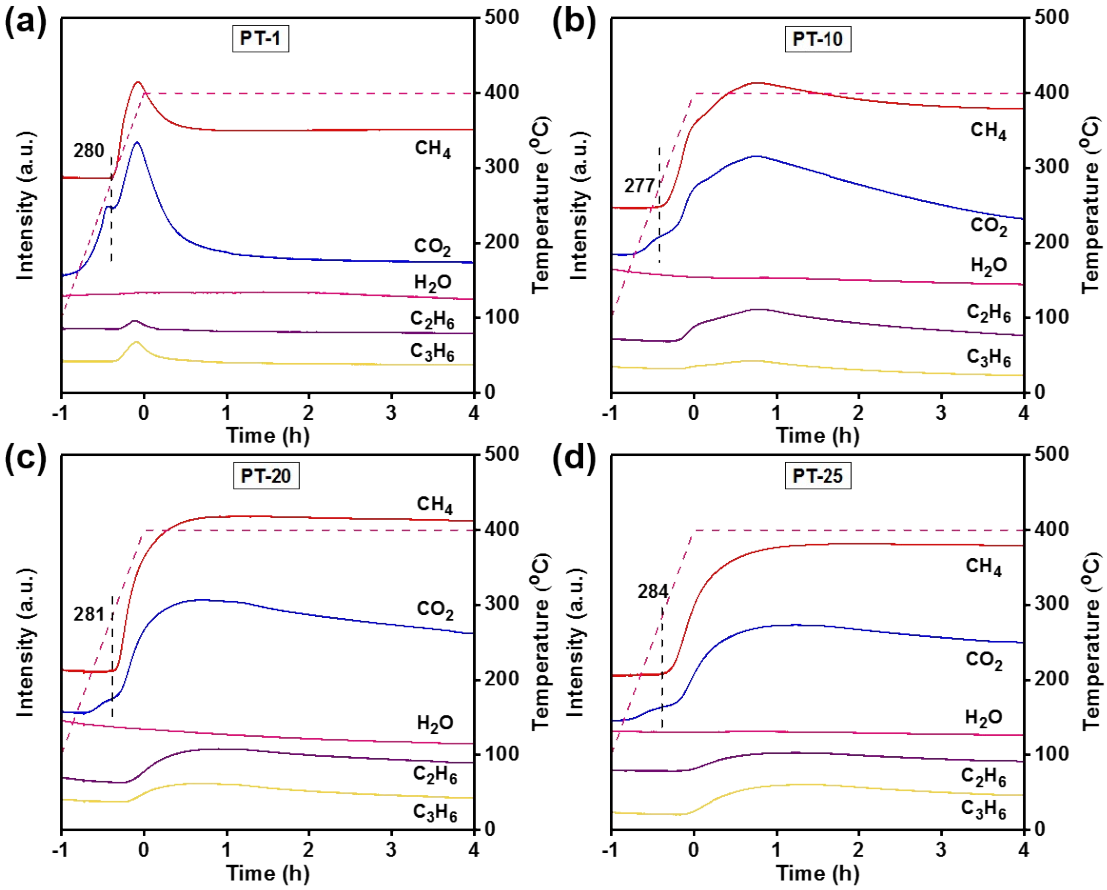

Figure S8. Time and temperature dependent TPSR diagrams during pretreatment processes under syngas atmosphere (H_2/CO=2) at (a) 1 bar, (b) 10 bar, (c) 20 bar and (d) 25 bar by *on-line* MS. Note that the time was counted 0 when the temperature reached 400 °C.

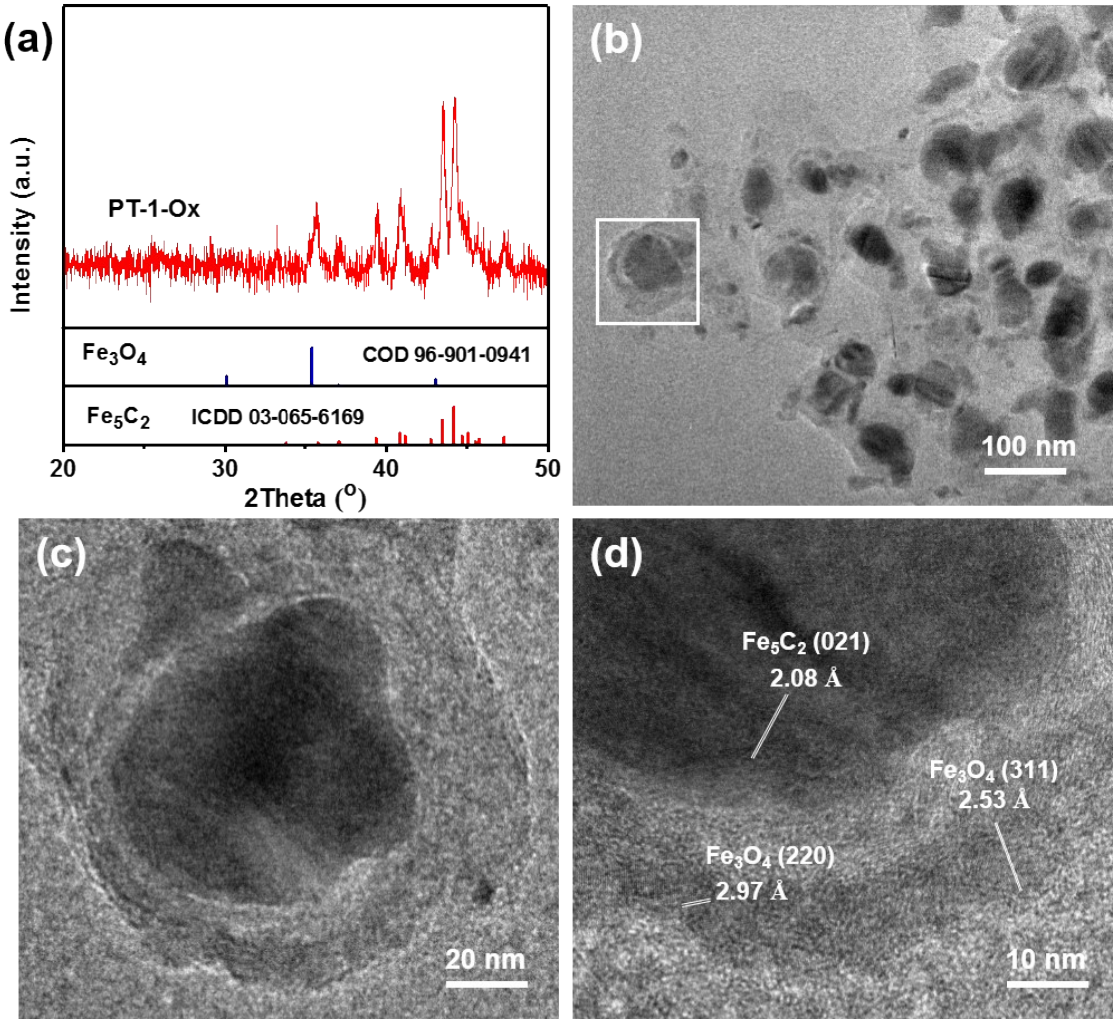

Figure S9. (a) XRD pattern and (b, c, d) TEM images of the PT-1-Ox catalyst. Note that the PT-1-Ox catalyst was obtained by oxidizing the PT-1 catalyst in 21%O_2/N_2 at 250 °C for 1 h.

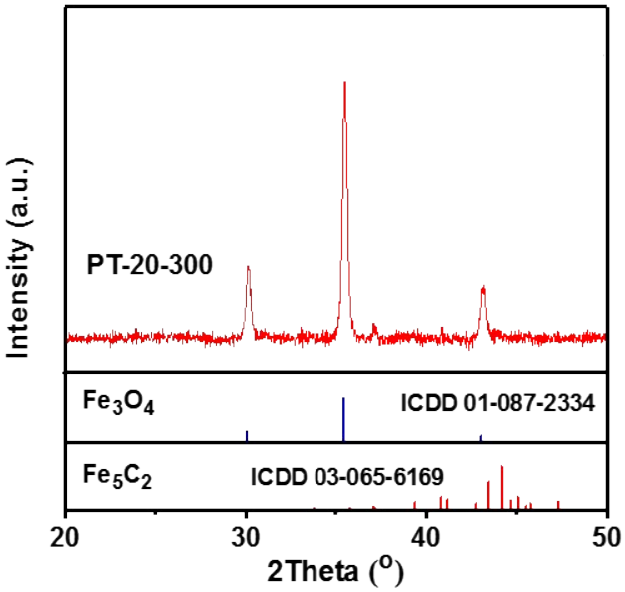

Figure S10. XRD pattern of the PT-20-300 catalyst. Note that the PT-20-300 catalyst was obtained by pretreating the Fe_3O_4 precursor in syngas (H_2/CO=2) at 300 °C and 20 bar for 4 h.

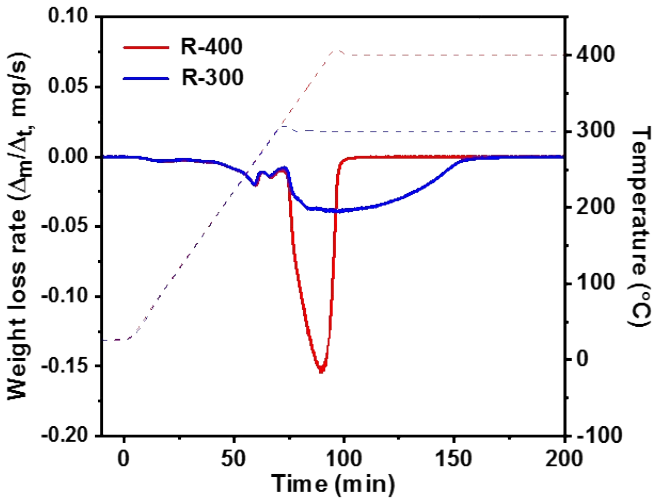

Figure S11. Weight loss rate of Fe_3O_4 as a function of time under H_2 atmosphere. Note that R-400 was heated at a rate of 5 °C min^{-1} to 400 °C by pretreating the Fe_3O_4 precursor in high-purity H_2 atmosphere. R-300 was heated to 300 °C in the same way.

To investigate the oxygen removal ability under different temperature-programed processes, the reduction experiments were conducted especially in H_2 atmosphere for excluding the interference of carbon diffusion and carbon deposition reactions in syngas atmosphere. The weight loss rate (Δ_m/Δ_t) that represents the hydrogenation removal rate of lattice oxygen of Fe_3O_4, was obtained on an intelligent gravimetric analyzer (IGA-100, Hiden Analytical). As shown in Figure S11, when temperature rises further above 300 °C, the weight loss rate is much higher than that at a constant temperature of 300 °C (R-300). A sharp peak of weight loss rate indicates a faster lattice oxygen removal kinetics under higher temperature.

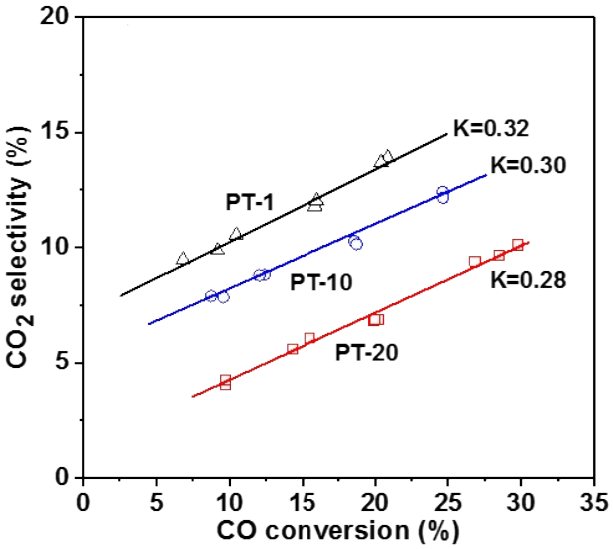

Figure S12. CO_2 selectivity as a functional of CO conversion. The CO conversion was varied by adjusting the flow rate of syngas in the range of 10~100 ml min^{-1}.

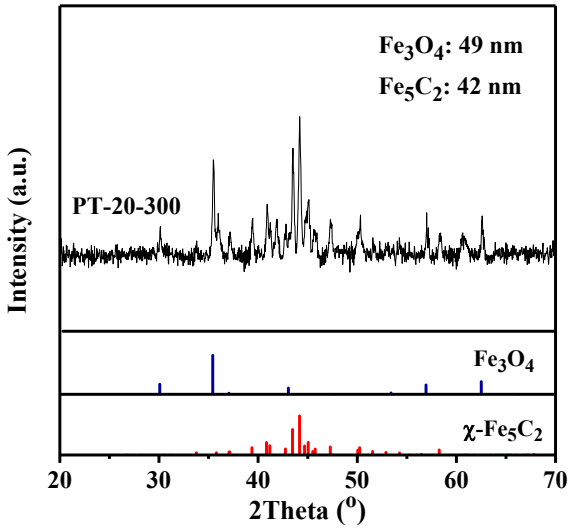

Figure S13. XRD pattern of the PT-20 catalyst after reaction at 300 ºC. Reaction condition: syngas (H_2/CO=2), 20 bar and 300 °C.

Table S1. Mössbauer fitted parameters of the pretreated PT-20 catalyst.

Catalysts	IS (mm s^{-1})	QS (mm s^{-1})	Hyperfine Field (T)	Γ (mm s^{-1})	Phases	Compositions (%)
PT-20	0.17	0.09	18.5	0.41	χ-Fe_5C_2 (I)	19.8
	0.26	0.04	21.8	0.50	χ-Fe_5C_2 (II)	23.5
	0.26	0.18	10.8	0.41	χ-Fe_5C_2 (III)	13.3
	0.26	-0.02	49.0	0.24	Fe_3O_4(A)	15.0
	0.65	-0.02	46.0	0.34	Fe_3O_4(B)	25.0
	0.20	1.08	-	0.39	spm Fe^{3+}	3.4

Table S2. Performance of representative Fe-based FTS catalysts over the reaction temperature range of 230~270 ºC in literature.

Sample	Conditions			CO Conv. [%]	Products Sel. [%][a]				Ref
	T [°C]	P [bar]	H_2/CO		CO_2	CH_4	$C_2^=$-$C_4^=$	C_{5+}	
PT-20	230	20	2	19	7	10	21	45	This work
Fe/α-Al_2O_3-H	250	1	1	2	43	22	31	1	1
Fe_2O_3-CO	270	13	0.7	86	46	6	N.G.	33[b]	2
FeCu/SiO_2	250	15	0.67	29	30	7[b]	9[b]	34[b]	3
FeCuNa/SiO_2	250	15	0.67	64	45	4[b]	13[b]	35[b]	3
FeSi	250	15	0.67	53	34	17[b]	23[b]	17[b]	4
FeKSi	260	15	2	57	46	7[b]	10[b]	31[b]	4
Fe-in-CNT	270	51	2	40	18	10	N.G.	24	5
Fe/NCNTs	270	20	1	45	21	11	4	60	6
χ-Fe_5C_2	270	30	2	24	10	14	17	35	7
in-Fe/CNT	270	20	2	86	39[b]	16[b]	N.G.	22[b]	8
ε-Fe_2C	235	23	1.5	15	5	16	N.G.	46	9

[a]Products selectivity (mol percentage) was normalized including CO_2. [b]Products distribution (mass percentage, wt%) was normalized including CO_2. N.G.: Not Given.

Table S3. The representative catalytic performance of PT-*x* catalysts.[a]

Sample	Temperature [ºC]	Gas flow [ml min^{-1}]	CO Conv. [%]	Product sel.[%]			
				CH_4	C_2–C_4	C_{5+}	CO_2
PT-1	250	20	94	12	29	28	31
PT-1	250	50	64	11	38	27	24
PT-20	250	20	50	8	35	43	14
PT-1	300	20	97	17	27	24	32
PT-20	300	20	96	11	34	26	29

[a]Reaction conditions: syngas (H_2/CO=2), 20 bar.

REFERENCES

(1) Zhou, X. P.; Ji, J.; Wang, D.; Duan, X. Z.; Qian, G.; Chen, D.; Zhou, X. G. *Chem. Commun.* 2015, **51**, 8853-8856.

(2) Luo, M. S.; Hamdeh, H.; Davis, B. H. *Catal. Today* 2009, **140**, 127-134.

(3) An, X.; Wu, B. S.; Wan, H. J.; Li, T. Z.; Tao, Z. C.; Xiang, H. W.; Li, Y. W. *Catal. Commun.* 2007, **8**, 1957-1962.

(4) Li, J. F.; Cheng, X. F.; Zhang, C. H.; Chang, Q.; Wang, J.; Wang, X. P.; Lv, Z. G.; Dong, W. S.; Yang, Y.; Li Y. W. *Appl. Catal. A-Gen.* 2016, **528**, 131-141.

(5) Chen, W.; Fan, Z. L.; Pan, X. L.; Bao, X. H. *J. Am. Chem. Soc.* 2008, **130**, 9414-9419.

(6) Li, Z. H.; Liu, R. J.; Xu, Y.; Ma, X. B. *Appl. Surf. Sci.* 2015, **347**, 643-650.

(7) Yang, C.; Zhao, H.; Hou, Y. L.; Ma, D. *J. Am. Chem. Soc.* 2012, **134**, 15814-15821.

(8) Abbaslou, R. M. M.; Tavassoli, A.; Soltan, J.; Dalai, A. K. *Appl. Catal. A-Gen.* 2009, **367**, 47-52.

(9) Wang, P.; Chen, W.; Chiang, F. K.; Dugulan, A. I.; Song, Y. J.; Pestman, R.; Zhang, K.; Yao, J. S.; Feng, B.; Miao, P.; Xu, W.; E Hensen, J. M. *Sci. Adv.* 2018, **4**, eaau2947.